HAL
open science

Cathodic driven coating delamination suppressed by inhibition of cation migration along Zn|polymer interface in atmospheric CO2

Viacheslav Shkirskiy, Matthias Uebel, Alina Maltseva, Grégory Lefèvre, Polina Volovitch, Michael Rohwerder

To cite this version:

Viacheslav Shkirskiy, Matthias Uebel, Alina Maltseva, Grégory Lefèvre, Polina Volovitch, et al.. Cathodic driven coating delamination suppressed by inhibition of cation migration along Zn|polymer interface in atmospheric CO2. npj Materials Degradation, 2019, 3, pp.2. 10.1038/s41529-018-0064-z . hal-02380908

HAL Id: hal-02380908

https://hal.science/hal-02380908v1

Submitted on 26 Nov 2019

HAL is a multi-disciplinary open access archive for the deposit and dissemination of scientific research documents, whether they are published or not. The documents may come from teaching and research institutions in France or abroad, or from public or private research centers.

L'archive ouverte pluridisciplinaire **HAL**, est destinée au dépôt et à la diffusion de documents scientifiques de niveau recherche, publiés ou non, émanant des établissements d'enseignement et de recherche français ou étrangers, des laboratoires publics ou privés.

npj | Materials Degradation

www.nature.com/npjmatdeg

ARTICLE OPEN

Cathodic driven coating delamination suppressed by inhibition of cation migration along Zn|polymer interface in atmospheric CO_2

Viacheslav Shkirskiy[1], Matthias Uebel[1], Alina Maltseva[2], Grégory Lefèvre[2], Polina Volovitch[2] and Michael Rohwerder[1]

The degradation of the Zn|polymer interface is inhibited by CO_2 gas in a humid environment. The inhibition mechanism varies greatly for different polymer matrices and depends on the affinity of the polymer to CO_2. Coatings based on polymers with high affinity to CO_2 such as polyacrylamide show high delamination rates due to the fast uptake of water. In this case, the cation transport that causes the initial pull down of potential for initiating the oxygen reduction reaction occurs via the polymer. Here CO_2 decreases water uptake due to competitive absorption into the polymer matrix, inhibiting the delamination rate. CO_2 can quickly reach the interface of polymers with functional groups with a low affinity to water and CO_2, such as polyvinyl butyral and polyvinyl alcohol. In this case, the inhibition of the delamination rate is achieved by a strong decrease in cation migration rate at the Zn|polymer interface accompanied by the formation of mixed hydrozincite/absorbed CO_2 layers on the ZnO surface underneath the polymers. Further experiments showed that the presence of CO_2 accelerates anion migration, suggesting an influence of CO_2 on the surface charge at the Zn|coating interface, thus affecting ion migration. Inhibition of cation migration has never been reported before and should be taken into account into the mechanism of cathodic-driven delamination on Zn under atmospheric conditions.

npj Materials Degradation (2019)3:2 ; https://doi.org/10.1038/s41529-018-0064-z

INTRODUCTION

Carbon dioxide (CO_2) is one of the most common gases present in any corrosive environment.[1] Extensive research in atmospheric corrosion on bare metals has showed that CO_2 strongly impacts the corrosion performance significantly, inhibiting degradation of many metals and their alloys.[1–3] In contrast, there is little information reported on the effect of CO_2 on the degradation of polymer-coated metal systems. A rare example of systematic studies on epoxy-coated Zn-based substrate for a wide range of 0–5 vol% of CO_2 revealed a more than 60% suppression of delamination propagation (i.e., disbonding of metal|polymer interface) under exposure even at a modest value of 0.5 vol% of CO_2.[4] In that work, the authors demonstrated the formation of a Zn carbonate species at the Zn interface, pointing out that there is penetration of the epoxy polymer by CO_2. It was proposed that the observed inhibition of the delamination process might be due to an inhibition of oxygen reduction at the interface. It is important to note that permeability of CO_2 might greatly vary for different polymers. From the research on CO_2/N_2 separation, it is known that the CO_2 permeability can be decreased if specific groups with high affinity to CO_2 adsorption are incorporated into the polymer matrix,[5–8] and this might restrict the access of CO_2 to the metal|polymer interface. For example, the introduction of amine,[9] tetrazole,[10] and thioamide[11] groups into the polymers with intrinsic porosity (PIM) decreased the CO_2 permeability by approximately 50% at 25 °C.

Once CO_2 reaches the Zn surface in humid O_2 containing atmosphere, Zn (hydroxy-)carbonate species are formed.[4,12–14] Stable in a wide pH range, these films are reported to reduce the rates of both cathodic and/or anodic reactions on the Zn surface.[12,14–18] Based on these findings, it was hypothesized that similar films at Zn|polymer interface inhibit O_2 reduction reaction at the delamination front, electrically balanced by the cation migration from the defect. In addition to the proposed reaction scheme, CO_2 gas can also influence cation migration in humid atmosphere as discussed recent work on ion migration on Al oxide.[19] Dissolution of CO_2 in a thin electrolyte layer on Al oxides causes a pH decrease that can alter the surface charge directly responsible for ion mobility. Similar effects could influence the delamination of the Zn|polymer interface. Nevertheless, they have never been considered in the literature.

The primary goal of this work was to detail the mechanism of CO_2 inhibition, namely to verify the possible influence of CO_2 on cation migration at the Zn|polymer interface in the cases where the polymer coating does not restrict CO_2 penetration. Two types of polymer were looked into based on the affinity of their functional groups to CO_2: of a low affinity, such as -OH (polyvinyl alcohol or PVA), and of a high affinity, such as $-NH_2$ (polyacrylamide or PAM), in comparison to polyvinyl butyral or PVB as a reference system widely used in delamination studies.[20,21] This follows on the second goal to uncover the possible influence of the polymer coating on the degradation of metal-coated systems in humid environments containing CO_2.

[1]Department of Interface Chemistry and Surface Engineering, Max-Planck-Institut für Eisenforschung GmbH, Max-Planck-Strasse 1, 40237 Düsseldorf, Germany and [2]Chimie ParisTech, PSL University, CNRS, Institut de Recherche de Chimie Paris, Paris 75005, France
Correspondence: Viacheslav Shkirskiy (viacheslav@shkirskiy.org) or Michael Rohwerder (rohwerder@mpie.de)
These authors contributed equally: Viacheslav Shkirskiy, Matthias Uebel.

Received: 11 June 2018 Accepted: 6 December 2018
Published online: 07 January 2019

Published in partnership with CSCP and USTB

nature partner journals

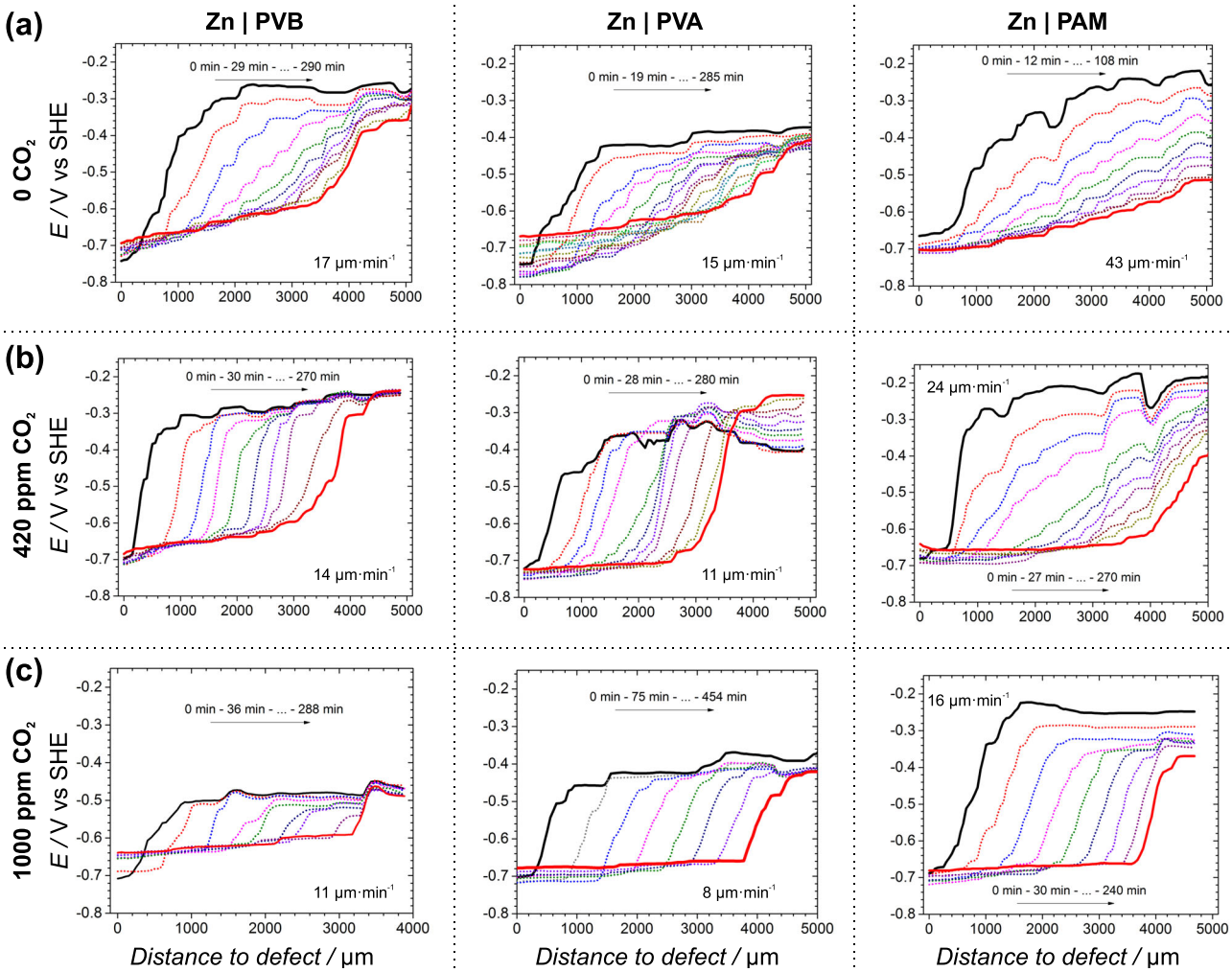

Fig. 1 Potential profiles of Zn|PVB, Zn|PVA, and Zn|PAM systems in humid air for CO_2 concentration of **a** 0 ppm, **b** 420 ppm, and **c** 1000 ppm at different exposure times after the addition of 0.5 M NaCl to the defect. The numbers in each graph show the average delamination rate in μm min^{-1}. Consult Fig. S5 for delamination kinetics

RESULTS

Evolution of potential profiles as a function of CO_2 concentration

Figure 1 demonstrates the evolution of potential profiles for all studied systems as a function of CO_2 concentration. All profiles show three distinct regions characteristic for a delaminating Zn|polymer interface.[22,23] The first region starts near the artificial defect at 0 μm and extends to the sharp increase of the potential. This reflects the delaminated and corroding Zn interface beneath the polymer with typical potential values of approximately −0.7 V vs. standard hydrogen electrode (SHE), which is close to the corrosion potential of zinc. The second region shows higher electrode potentials of about −0.3 to −0.5 V vs. SHE and corresponds to the intact Zn|polymer interface. The observed variations of the potential are most likely due to variations in the thickness of the zinc oxide layer and are in the range of potentials usually reported in literature for polymer-coated zinc.[22,24,25] The third region corresponds to the potential transition from the delaminated region to the intact interface.[26] The propagation of its position shows the progress of delamination. The gradual increase of the potential from 0 μm to the position of the delamination front corresponds to the Ohmic drop (*iR*, where *i* is the ionic current and *R* is the resistance for ion transport along the interface) due to a finite ionic conductivity of the interfacial liquid.[22,26] The ion transport between the defect site (net anode) and the delaminated interface and the delamination front (net) cathode counterbalances the electron flow from the defect site and thus closes the electric circuit.

Already at 0 min all curves shown in Fig. 1 have a sharp increase of the potential, pointing out partly delaminated Zn|polymer interfaces already at the beginning of the experiment. This can be explained by mechanically induced coating deadhesion during the generation of the artificial defect and the 10–15 min delay between the addition of 0.5 M NaCl to the defect and the first scan of scanning Kelvin probe (SKP) measurement.

The potential within the first region of the delamination profile, that is, the potential at the delaminated interface, tends to become flatter (i.e., with less Ohmic *iR* drop) with increasing CO_2 concentration for all coating systems (Fig. 1). Similar results were obtained for the Zn|epoxy-based coating in the work of Fürbeth and Stratmann.[4] This has to be due to a decrease of *iR*. It is conceivable that both *i* and *R* are decreasing. This will be discussed later in more detail.

The potential of the intact Zn|polymer interface remains nearly constant with time for Zn|PVB and Zn|PVA and the slight variations do not show any specific trend in Fig. 1. In contrast, this value gradually decreases for the Zn|PAM system during delamination measurements from −0.26 to −0.56 V vs. SHE, from −0.24 to −0.42 V vs. SHE, and from −0.28 to −0.38 V vs. SHE V at 0, 420, and 1000 ppm of CO_2 correspondingly. The difference in the absolute values decreases with O_2 content increase. This

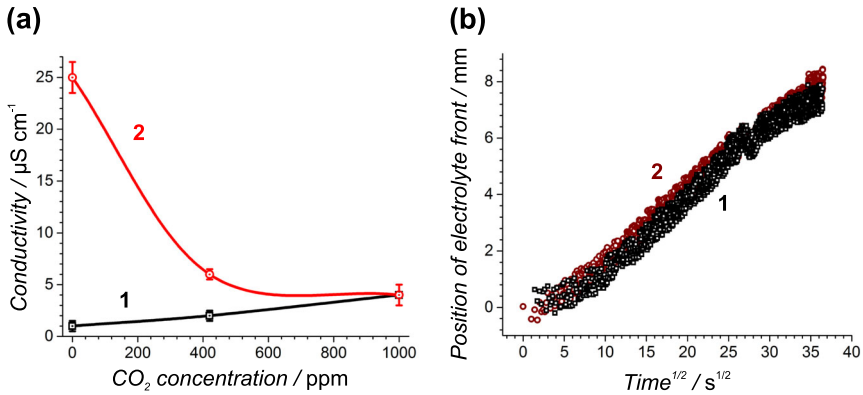

Fig. 2 **a** Conductivity of PAM coating (1) after 24 h exposure in humid atmosphere (σ_p) and (2) after the complete uptake of 0.5 M NaCl in PAM from the reservoir (σ) as a function of CO_2 concentration (see Fig. S2 for reference). **b** shows the kinetics of electrolyte propagation calculated by Eq. (3) in PAM for (1) 0 ppm and (2) 420 ppm of CO_2

steady decrease with time most likely is correlated with the electrolyte uptake into the hydrophilic PAM coating, for example, by an advancing diffusion of water which destabilizes the intact interface, which results in a change towards more active potentials.

The most remarkable observation from Fig. 1 concerns the influence of CO_2 on the steepness of the delamination front. For all studied systems, it becomes steeper with the increase of CO_2 concentration. This is the most pronounced for Zn|PAM interface with a clearly visible steep increase of potential in the presence of 420 and 1000 ppm of CO_2 which cannot be observed anymore at 0 ppm of CO_2 (Fig. 1a, right). This effect correlates with the inhibition of the delamination rate with CO_2 increase in Fig. 1.

The shape of this region is characterized by the distribution of cations on the border of the local galvanic element.[26] A smooth increase in potential at the delamination front can be indicative of significant cation migration rates comparable to the delamination rates already along the intact interface. The hypotheses about cation migration along Zn|PVB interface and electrolyte uptake into hydrophilic PAM matrix will be verified in the following sections.

Electrolyte uptake into the PAM polymer matrix in CO_2 humid atmosphere

The steady-state conductivity of the PAM polymer after its saturation at a relative humidity (RH) of 95% for 24 h gradually increases from 1 to 4 µS cm^{-1} with CO_2 concentration, which can be explained by the presence of soluble carbonates or carbonic acids within the polymer matrix (Fig. 2a, curve 1). These values reached the steady state after 4–6 h of exposure. For the reference, the measured conductivity of distilled water was approximately 5 times higher under similar CO_2 content. Then, 0.5 M NaCl was added to the reservoir. The PAM coating was completely saturated with electrolyte from the reservoir after 30 min of the experiment. Now the conductivity of the saturated PAM gradually decreases with the increase of CO_2 content, from 25 to 4 µS cm^{-1}. This signifies that the absorption of CO_2 into the PAM matrix decreases the total amount of absorbed electrolyte, probably due to a competitive H_2O/CO_2 adsorption on amine groups.

It is worth reminding that a hydrophobic PVB layer was on the top of every polymer coating, preventing a spreading of electrolyte from the reservoir onto the hydrophilic polymer layer (PAM). The experimental setup is depicted in Fig. S2. Separate experiments of PAM coating with and without PVB as a top layer demonstrated identical steady-state values of polymer conductivities after saturation in humid atmosphere, which were reached in both cases after 4–6 h independent of the CO_2 concentration. This fact discards the possible influence of the PVB top layer on the mass transport of CO_2 and H_2O.

Figure 2b shows the kinetics of electrolyte propagation for the cases of 0 ppm (curve 1) and 420 ppm (curve 2) of CO_2 calculated with Eq. (3) in the Methods section. The high rate of 600 µm min^{-1} of electrolyte propagation can be explained by the strong hydrophilic properties of PAM, referred to in the literature as a superabsorbent.[27] The electrolyte should propagate ahead of the delamination front since electrolyte propagation is significantly faster than the delamination rate. This can explain the smearing out of the delamination profiles in Fig. 1a, b for PAM and the decrease of the potential at intact Zn|polymer interface with time. This also correlates with the decrease of potential within the intact area of the PAM|Zn interface (far away from the delamination front) shown in Fig. 1a–c, which gets less pronounced with increasing CO_2 concentration.

An attempt was made to estimate electrolyte uptake into PAM in immersion experiments without artificial defect with electrochemical impedance spectroscopy (EIS). The first EIS spectrum after 5 min of immersion was identical to the spectrum of a bare Zn interface. Visual inspection showed wet deadhesion. This once again emphasizes the highly hydrophilic properties of the PAM layer.

The linear relation of electrolyte propagation in squared root of time coordinates in Fig. 2b suggests diffusion-controlled transport.[26] The identical behavior of kinetic curves 1 and 2 with different conductivity values at saturated conditions in Fig. 2a indicates identical mechanisms of electrolyte transport with a locking of some pathways in the presence of CO_2.

In contrast, conductivities of PVB and PVA polymers were below the detection limit of 0.01 µS cm^{-1} under all considered conditions. This discards the possible influence of electrolyte uptake into the polymer on the smearing out of the potential at the delamination front in Fig. 1 for these systems. The hypothesis of the role of cation migration at the Zn|polymer interface will be verified in the following.

Ion migration along the Zn|PVB interface

Experiments were carried out with a scanning Kelvin probe (SKP) in humid N_2 atmosphere in order to follow the migration of ions along the intact metal|coating interface. For this purpose, two different sample setups were prepared (see Figure S1), that either constituted a driving force for the migration of cations or for the migration of anions. The migration of cations is driven by providing a greater electrode potential at the Zn|PVB interface (intact coating) as compared to the metal|electrolyte interface (reservoir). Such an electrode potential difference is given for the sample setup Zn(reservoir)-Zn|PVB (intact coating). The potential

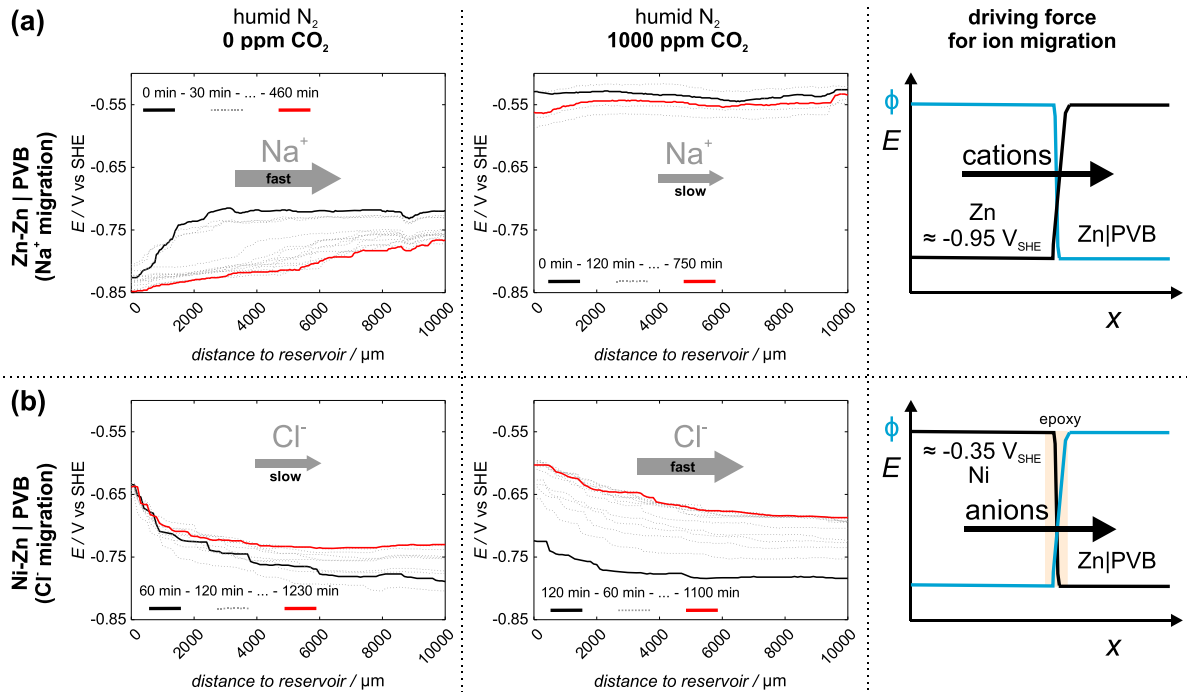

Fig. 3 Electrode potential profiles of **a** Zn-Zn|PVB and **b** Ni-Zn|PVB systems in humid N_2 atmosphere containing 0 or 1000 ppm of CO_2 after the addition of 0.5 M NaCl to the reservoir. Zn or Ni is used as a reservoir material, maintaining electrode potentials at the reservoir of approx. −0.95 V vs. SHE and −0.35 V vs. SHE, respectively. The corresponding electrode potential difference (note, the course of Galvani potential Φ at the polymer side of the interface is inverse to E, while at the metal side of the interface it is constant[28]) between the reservoir and the connected Zn|PVB interface creates a driving force either for cation migration (Zn reservoir) or anion migration (Ni reservoir) as indicated in the schemes on the right

difference has to be vice versa for driving the migration of anions, that is, higher electrode potential at the metal|electrolyte interface (reservoir) as compared to the Zn|PVB interface (intact coating). This was realized by using nickel as a metal at the reservoir, which is electrically coupled to the Zn|PVB (see Figure S1). This sample setup is denoted as Ni-Zn|PVB. The impact of atmospheric CO_2 concentration was investigated for both the migration of cations and the migration of anions.

Figure 3a shows the evolution of potential profiles for the Zn-Zn|PVB system in a humid N_2 atmosphere, aimed to follow cation migration along the intact Zn|PVB interface. Note, no delamination occurred during these experiments, since no oxygen reduction reaction takes place at the Zn|PVB interface in the absence of O_2. The observed decrease of the potential as a function of the distance to the reservoir filled with electrolyte is a consequence of cation migration. More precisely, the migration of cations in the electric field at the polymer side of the metal|polymer interface paired with electron flow at the metal side of the interface, that is, a dipole is migrating along the interface with positive charge at the polymer side of the interface and negative charge at the metal side, which is causing the decrease in potential. In comparison, the migration of anions at the polymer site of the metal|coating interface paired with a positive charge at the metal site will cause an increase of the electrode potential.

While the Galvani potential is constant in the metal, it is inverse to the electrode potential in the polymer, thus causing the migration of the ions (see sketches at the right side of Fig. 3 and in ref. [29]). The validation of this ion migration methodology is further explained in the experimental part.

Immediately after the addition of 0.5 M NaCl to the reservoir, its potential became approximately −0.95 V vs. SHE in both 0 and 1000 ppm of CO_2. This resulted in the potential difference with the higher potential at the intact Zn|PVB interface creating a driving force for a cation migration from the artificial defect (Fig. S5). The absolute values of potentials of intact Zn|polymer interfaces are lower than in air atmosphere shown in Fig. 1. This is caused by a strongly inhibited cathodic reaction due to significantly reduced O_2 content.

Figure 3a (left) shows a slightly smeared out potential jump at 0 ppm of CO_2, which moves away from the artificial defect with time. This reflects the position of the Na^+ cation migration front as mentioned in the Methods section. The initial rate of this transport of 18 µm min^{-1} is in the order of magnitude of the delamination rates of Zn|PVB and Zn|PVA systems in the absence of CO_2. This can explain the smeared out appearance of the potential jumps for the considered systems in absence of CO_2 (see Fig. 1a). The smearing out of potential profiles is, however, less pronounced for Zn|PVB and Zn|PVA systems than for Zn|PAM because the rate of cation migration is slower than the electrolyte uptake into the PAM matrix.

Remarkably, there is no such behavior at 1000 ppm of CO_2 during the whole duration of experiment in Fig. 3a (center figure). Nevertheless, the potential of the intact interface was clearly higher in comparison to the potential in the artificial defect, that is, there was a clear driving force for cation migration. This indicates a strong inhibition of cation transport in the presence of CO_2, which has never been reported before for a Zn|polymer interface. It is proposed that CO_2 increases the positive surface charge of the Zn|PVB interface, which leads to the inhibition of cation migration. If this is the case, then on the contrary, anion migration should be accelerated in CO_2 atmosphere.

This hypothesis is confirmed in Fig. 3b. The anion migration along the Zn|PVB interface in CO_2-free nitrogen atmosphere is strongly inhibited, showing no increase in potential profiles throughout the whole duration of the experiment. At the same time, a propagation of increasing potential due to the migration of anions is clearly observed in 1000 ppm of CO_2. It spreads along the x-axis causing a gradual increase of the potential at the Zn|PVB

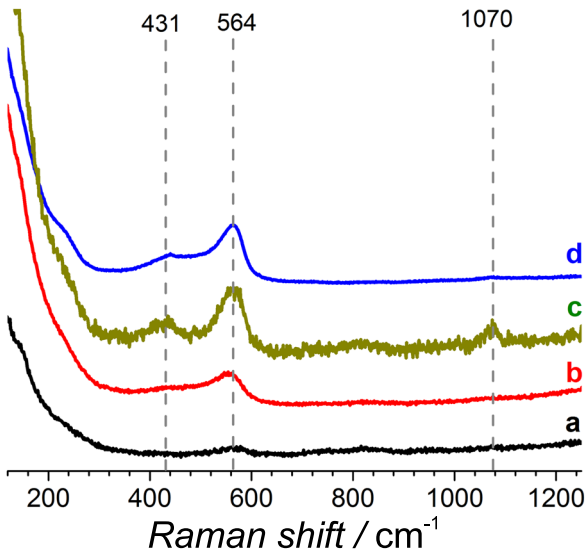

Fig. 4 Typical Raman spectra of Zn surface **a** immediately after the grinding procedure, **b**, **c** after the application of PVB layer and 24 h exposure to **b** 420 ppm and **c** 1000 ppm of CO_2 containing humid atmosphere, and **d** after application of PAM layer and 24 h exposure to 1000 ppm of CO_2 containing humid atmosphere

interface with some minor steps in potential apparent. This reflects a significantly smeared out anion migration front. Note that the concentration of Cl^- necessary for causing the observed increase in potential is very small, in the range of a percent of a monolayer, which is well below concentrations of chloride typically observed to induce corrosion at the interface.[29]

Surface observation of Zn interface in humid CO_2 containing atmosphere

Ex situ Raman spectroscopy was carried out in order to detect different species predominantly formed on the Zn substrate depending on the CO_2 concentration in the atmosphere and the type of polymer coating. The spectra obtained of freshly prepared Zn surface, seen in Fig. 4a, shows the absence of any surface corrosion products.

Application of a PVB polymer with exposure to 420 ppm of CO_2 humid atmospheres for 24 h causes the appearance of several peaks at 431 cm^{-1} and 564 cm^{-1} (Fig. 4b) attributed to the longitudinal optical phonons of ZnO.[30,31] The small peak at 1070 cm^{-1}, formed with the increase in CO_2 content to 1000 ppm (Fig. 4c), is characteristic for hydrozincite reflecting the ν_1 symmetric stretching mode of the carbonate unit.[32,33] Similar spectra were obtained for the Zn|PVA interface. In contrast, no carbonate-containing species were detected at the Zn|PAM interface after exposure to 1000 ppm of CO_2, but only the presence of ZnO was observed (Fig. 4d).

In situ attenuated total reflectance Fourier-transform infrared spectroscopy (ATR-FTIR) adsorption studies of CO_2 on ZnO as the main species at the Zn/polymer interface in humid environment were performed in order to gain fundamental insight into the mechanisms of CO_2 action. The adsorption of vapor water on ZnO during a preliminary 40 min exposure in the flow of humid air was observed (see Fig. S3). The last spectrum in this series was taken as a background and 5000 ppm of CO_2 was added to the air line.

This addition caused an immediate increase of peaks related to the vibrations of carbonates in Fig. 5a. The quantity of CO_2 was adjusted in separate experiments to observe a clear increase of carbonate bands. Peak decomposition of spectra after 10 and 40 min of exposure to CO_2 in the insets of Fig. 5a can be made with the initial rise of two peaks at 1500 cm^{-1} and 1410 cm^{-1} with following appearance of the peaks at 1548 and 1370 cm^{-1} and slight shift of the peak at 1500 to 1480 cm^{-1}.

The double peak in Fig. 5a after 10 min exposure is characteristic for the distorted CO_3^{2-} group (ν_3 frequency)[32,34] and in principle it can be assigned to the solid hydrozincite observed in Raman or CO_2 adsorbed on ZnO. In the last case, the observed splitting of $\Delta\nu_3 = 90\ cm^{-1}$ can be attributed to the monodentate form of adsorbed carbonate pointing out to the formation of a Zn-O-CO_2 bond.[33,35] With the increase of disorder due to the presence of structural water in hydrated or hydroxylated-water forms, the distorted crystal structure of the double CO_3^{2-} peak can be further split and/or slightly shifted,[12,14–17,36] as observed in Fig. 5a after 40 min exposure. The variation of the ratio between 1500 and 1480 cm^{-1} peak and 1410 cm^{-1} peak from 1.1 to 0.4, long with the change of the position of H-O-H bending vibrations from 1660 cm^{-1} to 1628 cm^{-1} in Fig. 5a, can be explained by complex ZnO surface transformation. This is due to the change of the ratio between adsorbed CO_2, precipitated hydrozincite, and transformation of hydrozincite structure itself.

The quantity of precipitated hydrozincite should be near constant with the decrease of CO_2 content in H_2O environment due to its low solubility, whereas the quantity of adsorbed CO_2 on ZnO should depend on CO_2 partial pressure due to the reversibility of the adsorption process. Data in Fig. 5b show the decrease of bonds at 1480 and 1410 cm^{-1} when CO_2 content was decreased from 5000 ppm to ambient 420 ppm. This suggests the removal of adsorbed CO_2. It is hence suggested that the observed effect of CO_2 on the delamination kinetics is an effect of adsorbed CO_2, as will be discussed in detail in the following.

DISCUSSION

The mechanism of CO_2 on the inhibition of the delamination of Zn|polymer systems directly depends on the polymer composition. If a polymer matrix such as PAM has a high affinity to CO_2, it restricts CO_2 penetration to the Zn|polymer interface. This was confirmed by post-mortem Raman analysis in Fig. 4d. Amine functional groups in the PAM polymer defined a high affinity to CO_2 of polymer matrix, and at the same time also to high hydrophilic properties, referred in the literature as a super-absorbent in respect to H_2O.[27] This caused NaCl electrolyte penetration into the PAM matrix from the reservoir, causing smearing of potential profiles at the delamination front, a decrease of potential at intact Zn|PAM interface, and a significant increase of delamination rates. In this case, the cation transport that causes the initial pull down of potential for initiating the oxygen reduction reaction occurs via the PAM polymer. Full coupling to the defect seems to require oxygen reduction reaction driven delamination that is still visible as a smeared out delamination front in the potential profiles. The inhibition effect of CO_2 consists in the decrease of the amounts of electrolyte uptake into PAM matrix, more likely due to a competitive sorption of CO_2 and H_2O on amine groups.

The second type of polymers possess a low affinity to carbonates, hence permitting relatively fast CO_2 transport through the polymer matrix and interaction with the Zn interface. This case has been already presented by Fürbeth and Stratmann,[4] who attributed the inhibition effect by CO_2 to the formation of protective Zn carbonate layers at the Zn interface. Different to the work by Fürbeth and Stratmann,[4] in our case the CO_2 content was significantly lower, and as a consequence, no significant amount of carbonate was found at the Zn interface. Raman spectra shown in Fig. 4b, c point out the presence of ZnO as the main species at the Zn|PVB interface, where CO_2 is mainly present in its adsorbed state.

It is hence suggested that the observed effect of CO_2 on the delamination kinetics is an effect of adsorbed CO_2 or rather its

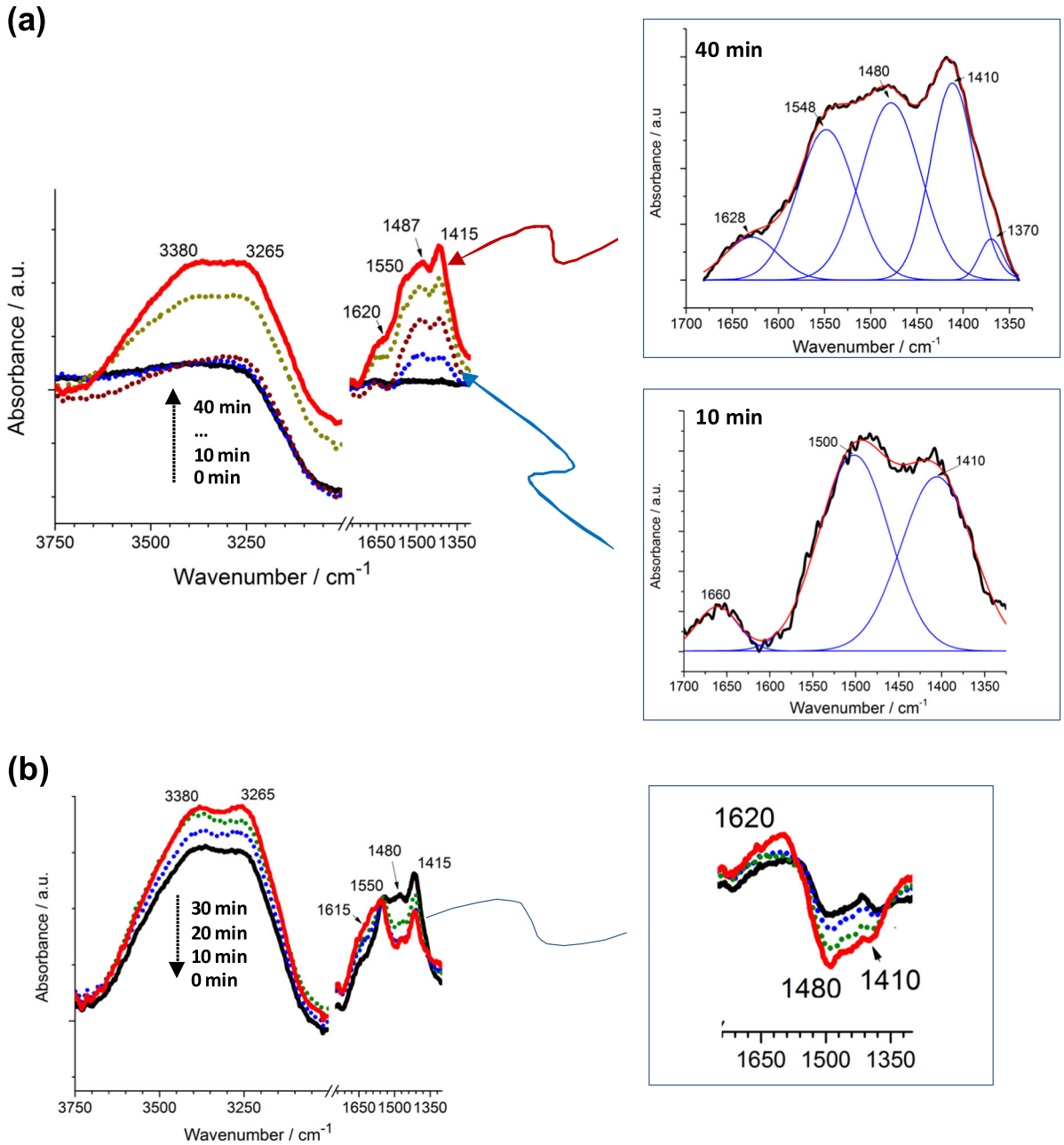

Fig. 5 Evolution of IR spectra of ZnO under the flow of humid air **a** after the addition of 5000 ppm CO_2 to the air line and then **b** the decrease to an ambient concentration of 420 ppm. Insets in **a** show Gaussian decomposition of peaks after 10 and 40 min of CO_2 addition. Inset in **b** shows spectra after the subtraction of the first spectrum at 0 min

effect on interfacial pH at the intact interface, which in turn results in different degrees of surface charging (Fig. 6).

The adsorption of carbonate has only a slight effect on the isoelectric point of zinc oxide, which is approximately 9, where adsorbed CO_2 may lead to a slight decrease to roughly 8.5.[37] This means that zinc oxide/hydroxide at the intact interface will be positively charged in any of the cases investigated here, but much more at higher CO_2 content than in CO_2-free atmosphere. In fact, CO_2 acidifies the pH of aqueous electrolyte from about pH 7 at 0 ppm of CO_2 to pH 5.2 in 1000 ppm of CO_2 as measured herein. It is known from the literature that the positive surface charge of ZnO increases from pH 7 to 5 because its zeta potential increases accordingly from +20 to +35 mV.[38] In turn, the increase of surface-positive charge will have an inhibitive effect on cation migration and accelerate anion migration, as is indeed observed in Fig. 3. As mentioned, similar effects of CO_2 gas on ion migration were already discussed recently for the case of ion mobility on alumina surfaces.[19] The crucial step for initiating the delamination process is ingress of cations, which results in the lowering of potential. In the follow-up steps, oxygen reduction sets in leading then to the degradation of the interface. Since the cation mobility at the intact interface is suppressed at higher CO_2 levels, significant current flow to the forefront of delamination is only possible along an already significantly delaminated interface, which causes the steep profile of the measured potential at the front. In the absence of CO_2, the much higher cation mobility allows also relatively high current flow along the intact or just partly degraded interface, which leads to the smeared out appearance of the potential profile at the front.

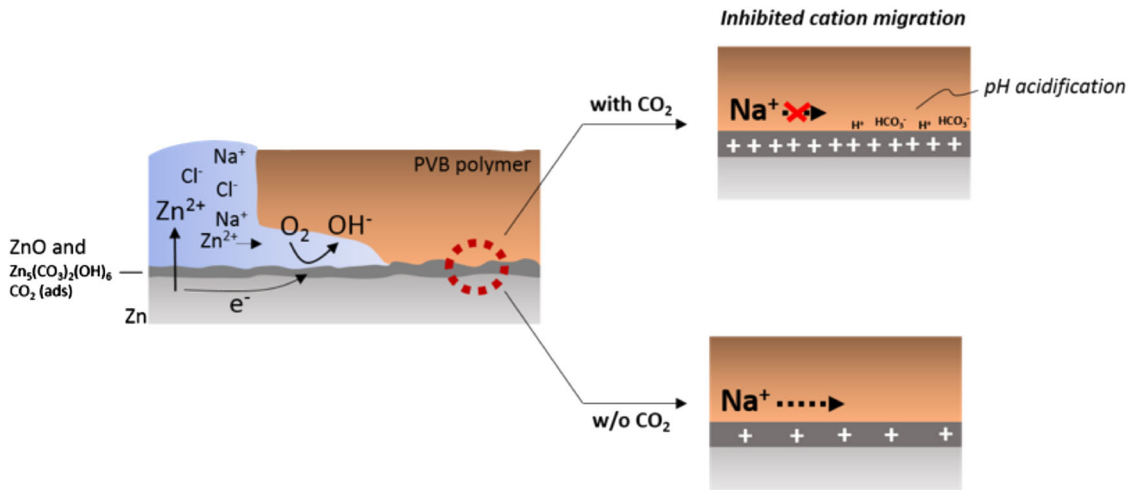

Fig. 6 Schematics of the new insight into the inhibition of Zn delamination by CO_2: inhibited cation migration caused by a pH acidification and thus increase of a positive surface charge of ZnO. Note, schematics does not show counter-negative charges compensating excess of positive charges on ZnO surface

Hence, we propose that it is indeed this inhibitive effect of CO_2 on the cation migration at the intact interface which is the main factor leading to the observed decrease in delamination rate at the here studied relatively low CO_2 concentrations.

Another observed effect is that the *iR* drop at the delaminated interface is decreasing with increasing CO_2 level. It is assumed that this might be due to the precipitation of hydroxyzincite observed in Fig. 4 at this corroding interface in the presence of higher levels of CO_2. Hydroxyzincite is known to show a higher hydrophilicity than zinc oxide or hydroxy/oxide.[39] This might lead to a better wetting of the surface at the delaminated interface by electrolyte and thus also to higher ionic conductivity. This would thus lower the *iR* drop at the delaminated interface. It is also possible that the oxygen reduction reaction on the hydrozincite is lower than on zinc oxide, therefore causing a decrease also of the net cathodic current density at the delaminated interface.

Remarkably, the effect of CO_2 inhibition of cation migration rates was well pronounced at near ambient CO_2 content of 0–1000 ppm. If not fixed intentionally, these CO_2 variations can easily occur in any corrosion environment. This signifies that any interpretations of delamination curves should be taken with caution of CO_2 impact on delamination mechanisms.

In summary, CO_2 inhibits the degradation of the Zn|polymer interface in a humid atmosphere while the mechanism of its action strongly depends on the chemical composition of the polymer. Polymers with high affinity to CO_2, such as PAM, restrict CO_2 access to the Zn|polymer interface. In this case, the cation transport that causes the initial pull down of potential for initiating the oxygen reduction reaction occurs via the polymer. Hence, the inhibition action is defined by CO_2 absorption into the hydrophilic PAM polymer that also decreases electrolyte uptake, especially at the Zn|polymer interface, and thus contributes to the decline of the delamination rate.

Polymers with a low affinity to CO_2, such as PVB and PVA, permit CO_2 penetration to the Zn|polymer interface where it mainly adsorbs in the form of monodentate CO_2 complexes. The presence of this CO_2 causes strong inhibition of cation migration along the Zn|polymer interface, which has never been reported before. Ion migration experiments showed that at the same time CO_2 caused acceleration of anion migration along the intact Zn|PVB interface. This correlates well with the fact that CO_2 alters the surface charge of Zn interface. Inhibition of cation migration is well pronounced already at natural CO_2 concentration, which implies it to be an important parameter of the delamination mechanism of Zn|polymer delamination under atmospheric conditions.

METHODS

Coatings preparation

All solutions were prepared in either ultra-pure water (ELGA LabWater purification system) with a conductivity of < 0.055 μS cm^{-1} or high-purity ethanol (Sigma-Alrdich, >99.8% purity). All chemicals had analytical purity grade and were supplied by Sigma-Aldrich.

Zn plates of 1.0 cm × 1.8 cm × 0.5 cm (GoodFellow GmbH, 99.95% purity) were grinded with SiC emery papers up to P4000 with tap water, and rinsed with EtOH and distilled water afterwards. The edge of a 0.5 cm × 1.0 cm Zn sample was covered with Gamry electroplating tape (3 M 470, 0.18 mm thick). The solution of the desired polymer (5 w/w% of PVB in ethanol or 5 w/w% PVA in water or 2.5 w/w% PAM in water) was applied to the sample surface and placed in a spin coater machine. A velocity of 2000 rotations per minute (rpm) for PVB and PVA, and 4000 rpm for PAM for 30 s was employed two times with 30 s interval. The values of velocity were adapted to provide similar coating thickness. Then, the sample was placed in an oven at 80 °C for ~5 min. In the case of PVB polymer coating the procedure was repeated 3 times. For more hydrophilic PVA and PAM polymers, the procedure was repeated 2 times with the application of a hydrophobic PVB layer on top. In this way, the drop of electrolyte could stick to the edges of polymer coatings. The PVB top coating did not restrict the mass transport of CO_2 and H_2O, later proven by electrolyte uptake measurements. The final coatings were near transparent, with the average thickness of ~10 μm measured with a height-controlled SK P system (Fig. S5). The Gamry electroplating tape was gently removed after the application of the polymer to create the artificial defect. An applied mechanical force caused a loss of adhesion between the polymer and the Zn metal 1–2 mm long from the defect visible from the potential profiles at 0 min seen in Fig. 1. The separate experiments showed that the polarization curves of Zn surfaces in 0.5 M NaCl were identical before and after the application of Gamry electroplating plate. It excludes the possible influence of the glue from the adhesive tape on the electrochemical behavior of Zn surface in the artificial defect. The edges of the sample in the artificial defect were covered with two components X60 superglue (Hottinger Baldwin Messtechnik GmbH) to create a reservoir for the corrosive electrolyte.

Delamination studies: SKP setup

The detailed description of the SKP) used in this work can be found elsewhere.[40] Briefly, it is based on the vibrating condenser method. A paraffin-coated SKP-tip (home-made Ni(80)/Cr(20) plane-ended with ~100 μm diameter[41]) is positioned tens of micrometer above the sample surface under the atmospheric conditions and brought into the electrical contact with it. The establishment of the equilibrium of the Fermi levels within the two metals results in a surface charging of sample and probe

causing a Volta potential difference between the needle and the surface. A current is induced by vibrating the needle perpendicular to the sample surface and compensated by application of an external bias voltage identical to the Volta potential difference between the sample and the needle. Numerous studies demonstrated that the corrosion potential (E_{corr}) of intact metal|polymer interfaces (Eq. 1) and delaminated metal|polymer interfaces (Eq. 2) are linearly related to the measured Volta potential difference ($\Delta\psi$):[42]

$$E_{corr} = \text{const} + \Delta\psi, \quad (1)$$

$$E_{corr} = \text{const} + \Delta\varphi + \Delta\psi, \quad (2)$$

where $\Delta\varphi$ is the Donnan potential. The appearance of Donnan potential results from an ion-selective incorporation of charged species from the electrolyte into the polymeric membrane.[42] The exact value of the corrosion potential was calibrated vs. $Cu/CuSO_4$ just before the experiment in the desired atmospheric conditions and regularly checked throughout the experiments to verify its stability. The electrode potentials were referred to the SHE. The calibrated potentials of actively corroding Zn metal interfaces beneath all mentioned polymers were similar to the uncovered Zn surface, indicating negligible Donnan potentials.

A constant air flow supplied by an aquarium pump (Aquaflow Technology AAP-301S) was passed through two bottles of aqueous solutions maintained at 95 ± 2% RH in an SKP chamber. The use of an aqueous suspension of $Ca(OH)_2$ to capture ambient CO_2,[43] tap water, and over saturated Na_2CO_3 solution with a constant addition of 5 M H_2SO_4 guaranteed 5 ± 5, 420 ± 40, and 1000 ± 90 ppm of CO_2 in the SKP chamber. Less than 1000 ppm CO_2 concentration was monitored with a CO_2 measuring instrument CM100 (Voltcraft) and more than 1000 ppm with a CO_2 transmitter instrument GMT220 (Vaisala).

Coated Zn samples with the artificial defect were kept for 24 h in an SKP chamber at given conditions prior to each experiment to guarantee the water saturation of the polymer, removing the possible influence of electrostatic charges on SKP measurement along with the saturation of Zn interface with O_2 and CO_2. Then, approximately 20 mL of 0.5 M NaCl solution was added to the artificial defect to initiate the delamination. After 10–15 min, line scans of Volta potential difference of the Zn|polymer interface were made perpendicular starting approximately 1 mm away from the artificial defect.

Ion transport along the Zn|polymer interface

A setup identical to the one described for the delamination experiments using SKP was employed to follow the migration of cations and anions along the Zn|PVB interface. For the investigation of cation migration, a Zn-Zn|PVB sample setup (Zn reservoir connected to PVB-coated Zn) was fabricated identical to the ones used for the delamination experiments described above. This provided the required potential gradient to drive cation migration[44] with lower potential values of −0.95 V vs. SHE in the reservoir relative to the intact Zn|PVB interface of −0.75 to −0.55 V vs. SHE depending on the CO_2 concentration.

For the investigation of anion migration, a Ni-Zn|PVB sample setup (Ni reservoir connected to PVB-coated Zn) was prepared. Here, a Zn sheet was glued to the Ni metal sheet with two epoxy-component X60 superglue with a 3 mm gap, filled with epoxy, between the two metals (Fig. S1). The physical separation of Ni and Zn was made to avoid lowering the potential in the Ni defect due to galvanic coupling with Zn (which would then prevent the higher potential in the defect, required for driving anions into the interface); however, electronic coupling was ensured by connecting both metals on the back side with a copper tape. The surface was mechanically grinded with SiC emery papers up to P4000 with tap water. Then, a Zn sheet was attached at the bottom of the sample to avoid a potential influence from the steel support of the SKP sample holder in the gap area (as this may also prevent anion migration), and to provide mechanical support to the Ni–epoxy–Zn connection. Identical to the preparation of Zn-Zn|PVB reservoir, the Ni including ~1 mm of the epoxy barrier was covered with adhesive tape. The PVB layer was applied on the Ni–epoxy–Zn surface in the spin coater. The adhesive tape was removed and edges of Ni were covered with epoxy-based superglue to create the reservoir suitable for electrolyte addition. The potential at the Ni defect had values of approx. −0.35 V vs. SHE during the whole experiment after the addition of electrolyte to the reservoir. This ensured a higher potential in the reservoir as compared to the intact Zn|PVB interface, providing a driving force for anion migration.[37]

The coated samples were kept for 24 h in N_2 humid atmosphere with 0 or 1000 ppm of CO_2 to exclude any influence of an oxygen reduction-driven delamination on the SKP profiles. Then, approximately 20 mL of 0.5 M NaCl solution was added to the reservoir. SKP scans were made starting approximately 1–2 mm away from the reservoir in both anion and cation migration experiments. Ion migration along the Zn|PVB interface initiated by galvanic coupling between reservoir and Zn|PVB interface caused an according modification of the measured potential profile, measured by SKP. This pulled the potential at the migrated region towards the one of their origin in the reservoir serving as an indication of ion propagation.

Ion transport through the polymer

It is commonly accepted that the cation migration along the Zn|polymer interface is faster than electrolyte penetration through a bulk polymer in the case of hydrophobic and slightly hydrophilic polymers[45,46] such as PVB and PAM. In contrast, the PAM polymer possesses hydrophilic properties and is even sometimes referred to as superabsorbent in the literature[27] emphasizing its high affinity to water. A home-made setup (Fig. S2) was built to verify if an electrolyte from the reservoir can penetrate into PAM bulk polymer. The results were compared to PVB and PVA coatings.

In the setup two silver wires with 1.0 mm diameter and 1.0 cm length were imbedded in resin made of two components X60 superglue (Hottinger Baldwin Messtechnik GmbH) of 2.0 cm × 1.0 cm size parallel to each other on the distance of 0.5 and 1.8 cm from edge of the resin. The Ag wires in resin were grinded to have a flat surface. The exposed area of each wire (A) was 0.10 ± 0.02 cm^2. A procedure identical to the polymer deposition on the Zn sample was used to apply a polymer layer and create a defect with a reservoir positioned 0.5 cm before the Ag wire as shown in Fig. 1. A home-made Arduino-based ohmmeter with external 1 V power supply piloted with Python script was used to continuously measure the resistance (R) between two wires in the range of 10 kΩ to 50 MΩ with 2% error. The identical system described before was used to maintain 95% RH and vary CO_2 concentration in the range of 0–1000 ppm. The detection limit for conductivity measurements in this setup was 0.01 μS cm^{-1}.

Each polymer coating was kept for 24 h in humid atmosphere to have the identical conditions to those of the delamination experiments. The measured resistance was used to define the conductivity of the polymer (σ_p). Then, 20 ml of 0.5 M NaCl was added to the reservoir and the dynamically changing value of the resistance was measured continuously until it reached a stable value after approximately 30 min. The measured final resistance was used to calculate the conductivity of the polymer saturated with the electrolyte (σ). Assuming homogeneous electrolyte penetration, the current position of the electrolyte front inside the polymer ($x(t)$) was calculated as:

$$x(t) = (R(t=0) - R(t))/\left(\sigma_p^{-1} - \sigma^{-1}\right). \quad (3)$$

Some experiments were done with the continuous measurement of resistance and with 15 min intervals between measurements giving similar results. This discards the possible influence of applied potential during resistance measurements on the electrolyte penetration. Every experiment was repeated at least two times.

Adsorption of CO_2 on ZnO: in situ ATR-FTIR

The adsorption of CO_2 on ZnO (nanopowder < 100 nm particle size, Sigma-Aldrich) was followed using infrared (IR) spectroscopy in the ATR mode. The ZnO film was deposited directly on the ATR crystal as described elsewhere.[47] Shortly, an aliquot of 1 μL of the ZnO suspension (4.5 g L^{-1}) in nitrogen-purged solution was pipetted onto the crystal and dried under a flow of nitrogen. Then the background was recorded. A pike flow cell[32] was used to deliver the air with 95% RH with ambient 420 or 5000 ppm concentration of CO_2. Humidity and CO_2 content were controlled with an equipment identical to the delamination studies using SKP described before. The evolution of the CO_2 adsorption on ZnO was followed by the acquisition of IR spectra every 3 min after the beginning of the experiment. Infrared spectra were measured with a Thermo Scientific Nicolet 6700 FTIR spectrometer equipped with a mercury cadmium telluride detector cooled at 77 K by liquid nitrogen. Spectral resolution was 4 cm^{-1}, and the spectra were averaged from 256 scans. The ATR accessory was a horizontal ZnSe crystal coated with diamond (A = 2.54 mm^2) with single reflection and an angle of incidence of 45° (Smart Miracle from PIKE). OMNIC software was used for the data collection and OriginLab software for the peak deconvolution.

Ex situ observation of Zn|polymer interface with Raman spectroscopy

The Zn surface was characterized by Raman spectroscopy immediately after grinding and after the exposure to CO_2 humid environments preceding the mechanical removal of the polymer with a scalpel. Raman spectra were recorded on Renishaw Confocal Raman Microscope, using the green laser (doubled Nd:YAG, 532 nm) with power of 10 mW. Illumination and detection were performed through a microscope objective Leica of ×5, ×20, and ×50 magnification factors and numerical aperture (NA) of 0.12, 0.40 and 0.75 respectively with the exposure time of 10 sec.

DATA AVAILABILITY

The data that support the findings of this study are available from the corresponding authors upon reasonable request.

ACKNOWLEDGEMENTS

V. Shkirskiy and M. Uebel gratefully acknowledge the German Academic Exchange Service (DAAD) and DFG SPP 1568 "Design and Generic Principles of Self-Healing Materials" correspondingly for the financial support, and I. Haugland-Gosling for proofreading and correcting this manuscript.

AUTHOR CONTRIBUTIONS

V.S. and M.U. carried out the delamination experiments using SKP, including sample preparation, CO_2, and humidity control system setup and processing of data. V.S. carried out the measurements on electrolyte penetration through polymer coating. M.U. carried out ion migration experiments. A.M. and V.S. carried out Raman experiments, V.S. and G.L. carried out in situ FTIR experiments. V.S., P.V., A.M., and G.V. contributed to the interpretation of spectroscopic data. V.S., M.R., and M.U. wrote the paper, all authors contributed to the proof reading. P.V. first proposed the idea of using the polymer of different polarities to see the effect of CO_2. M.R. determined the scientific course of the work, supervised, and coordinated the overall project.

ADDITIONAL INFORMATION

Supplementary information accompanies the paper on the *npj Materials Degradation* website (https://doi.org/10.1038/s41529-018-0064-z).

Competing interests: The authors declare no competing interests.

Publisher's note: Springer Nature remains neutral with regard to jurisdictional claims in published maps and institutional affiliations.

REFERENCES

1. Schaller, R. F., Jove-Colon, C. F., Taylor, J. M. & Schindelholz, E. J. The controlling role of sodium and carbonate on the atmospheric corrosion rate of aluminum. *Npj Mater. Degrad.* **20**, 1–8 (2017).
2. Cole, I. Recent progress and required developments in atmospheric corrosion of galvanised steel and zinc. *Materials* **10**, 1288–1300 (2017).
3. LeBozec, N. et al. Effect of carbon dioxide on the atmospheric corrosion of Zn-Mg-Al coated steel. *Corros. Sci.* **74**, 379–386 (2013).
4. Fürbeth, W. & Stratmann, M. The delamination of polymeric coatings from electrogalvanised steel—a mechanistic approach. Part 3: delamination kinetics and influence of CO_2. *Corros. Sci.* **43**, 207–227 (2001).
5. Kim, S. & Lee, Y. M. High performance polymer membranes for CO_2 separation. *Curr. Opin. Chem. Eng.* **2**, 238–244 (2013).
6. Brunetti, A., Scura, F., Barbieri, G. & Drioli, E. Membrane technologies for CO_2 separation. *J. Membr. Sci.* **359**, 115–125 (2010).
7. Bernardo, P., Drioli, E. & Golemme, G. Membrane gas separation: a review/state of the art. *Ind. Eng. Chem. Res.* **48**, 4638–4663 (2009).
8. Tanaka, K., Okamoto, K. I. Structure and transport properties of polyimides as materials for gas and vapor membrane separation. *Mater. Sci. Membr. Gas Vap. Sep*. 271–291 (2006).
9. Mason, C. R. et al. Enhancement of CO_2 affinity in a polymer of intrinsic microporosity by amine modification. *Macromolecules* **47**, 1021–1029 (2014).
10. Du, N. et al. Polymer nanosieve membranes for CO_2-capture applications. *Nat. Mater.* **10**, 372–375 (2011).
11. Mason, C. R. et al. Polymer of intrinsic microporosity incorporating thioamide functionality: preparation and gas transport properties. *Macromolecules* **44**, 6471–6479 (2011).
12. Falk, T., Svensson, J.-E. & Johansson, L.-G. The Influence of CO_2 and NaCl on the atmospheric corrosion of zinc. *J. Electrochem. Soc.* **145**, 2993–2999 (1998).
13. Lindström, R., Svensson, J.-E. & Johansson, L.-G. The atmospheric corrosion of zinc in the presence of NaCl—the influence of carbon dioxide and temperature. *J. Electrochem. Soc.* **147**, 1751–1757 (2000).
14. Falk, T., Svensson, J.-E. & Johansson, L.-G. The role of carbon dioxide in the atmospheric corrosion of zinc. *J. Electrochem. Soc.* **145**, 39–44 (1998).
15. Laska, Ca et al. Effect of hydrogen carbonate and chloride on zinc corrosion investigated by a scanning flow cell system. *Electrochim. Acta* **159**, 198–209 (2015).
16. Yoo, J. D., Ogle, K. & Volovitch, P. The effect of synthetic zinc corrosion products on corrosion of electrogalvanized steel. II. Zinc reactivity and galvanic coupling zinc/steel in presence of zinc corrosion products. *Corros. Sci.* **83**, 32–37 (2014).
17. Yoo, J. D., Volovitch, P., Abdel Aal, A., Allely, C. & Ogle, K. The effect of an artificially synthesized simonkolleite layer on the corrosion of electrogalvanized steel. *Corros. Sci.* **70**, 1–10 (2013).
18. Yoo, J. D., Ogle, K. & Volovitch, P. The effect of synthetic zinc corrosion products on corrosion of electrogalvanized steel. II. Zinc reactivity and galvanic coupling zinc/steel in presence of zinc corrosion products. *Corros. Sci* **83**, 32–37 (2014).
19. Salgin, B., Hamou, R. F. & Rohwerder, M. Monitoring surface ion mobility on aluminum oxide: effect of chemical pretreatments. *Electrochim. Acta* **110**, 526–533 (2013).
20. Vimalanandan, A. et al. Redox-responsive self-healing for corrosion protection. *Adv. Mater.* **25**, 6980–6984 (2013).
21. Williams, G. & McMurray, H. N. Anion-exchange inhibition of filiform corrosion on organic coated AA2024-T3 aluminum alloy by hydrotalcite-like pigments. *Electrochem. Solid-State Lett.* **6**, B9–B11 (2003).
22. Fürbeth, W. & Stratmann, M. The delamination of polymeric coatings from electrogalvanised steel-a mechanistic approach.-Part 1: delamination from a defect with intact zinc layer. *Corros. Sci.* **43**, 207–227 (2001).
23. Nazarov, A., Prosek, T. & Thierry, D. Application of EIS and SKP methods for the study of the zinc/polymer interface. *Electrochim. Acta* **53**, 7531–7538 (2008).
24. Tran, T. H. et al. Regenerative nano-hybrid coating tailored for autonomous corrosion protection. *Adv. Mater.* **27**, 3825–3830 (2015).
25. Nazarov, A., Diler, E., Persson, D. & Thierry, D. Electrochemical and corrosion properties of ZnO/Zn electrode in atmospheric environments. *J. Electroanal. Chem.* **737**, 129–140 (2015).
26. Leng, A., Streckel, H. & Stratmann, M. The delamination of polymeric coatings from steel. Part 2: first stage of delamination, effect of type and concentration of cations on delamination, chemical analysis of the interface. *Corros. Sci.* **41**, 579–597 (1999).
27. Liu, H., Bu, Y., Sanjayan, J. G., Nazari, A. & Shen, Z. Suitability of polyacrylamide superabsorbent polymers as the internal curing agent of well cement. *Constr. Build. Mater.* **112**, 253–260 (2016).
28. Rohwerder, M. in *Reference Module in Chemistry, Molecular Sciences and Chemical Engineering* 414–422 (Elsevier, Amsterdam, 2018).
29. Fuente, D. De. La, Flores, S. & Morcillo, M. Deterioration of paint systems applied on zinc substrates contaminated with soluble salts. *Prog. Org. Coat.* **41**, 183–190 (2001).
30. Bouchard, M. & Smith, D. C. Catalogue of 45 reference Raman spectra of minerals concerning research in art history or archaeology, especially on corroded metals and coloured glass. *Spectrochim. Acta* **59**, 2247–2266 (2003).
31. Azmat, N. S., Ralston, K. D., Muddle, B. C. & Cole, I. S. Corrosion of Zn under acidified marine droplets. *Corros. Sci.* **53**, 1604–1615 (2011).
32. Lefèvre, G. In situ Fourier-transform infrared spectroscopy studies of inorganic ions adsorption on metal oxides and hydroxides. *Adv. Colloid Interface Sci.* **107**, 109–123 (2004).
33. Turianicová, E.et al. Obut, CO2 utilization for fast preparation of nanocrystalline hydrozincite. *J. CO2 Util.* **16**, 328–335 (2016).
34. Wijnja, H. & Schulthess, C. P. ATR–FTIR and DRIFT spectroscopy of carbonate species at the aged γ-Al2O3/water interface. *Spectrochim. Acta Part A* **55**, 861–872 (1999).
35. Bitenc, M., Marinsek, M. & Crnjak Orel, Z. Preparation and characterization of zinc hydroxide carbonate and porous zinc oxide particles. *J. Eur. Ceram. Soc.* **28**, 2915–2921 (2008).
36. Yoo, J. D., Ogle, K. & Volovitch, P. The effect of synthetic zinc corrosion products on corrosion of electrogalvanized steel: I. Cathodic reactivity under zinc corrosion products. *Corros. Sci.* **81**, 11–20 (2014).
37. Hausbrand, R., Stratmann, M. & Rohwerder, M. The physical meaning of electrode potentials at metal surfaces and polymer/metal interfaces: consequences for delamination. *J. Electrochem. Soc.* **155**, C369–C379 (2008).
38. Muster, T. H. & Cole, I. S. The protective nature of passivation films on zinc: surface charge. *Corros. Sci.* **46**, 2319–2335 (2004).
39. Muster, T. H., Aaron, N. K. & Cole, I. S. The protective nature of passivation films on zinc: wetting and surface charge. *Corros. Sci.* **46**, 2337–2354 (2004).

40. Frankel, G. S. et al. Potential control under thin aqueous layers using a Kelvin probe. *Corros. Sci.* **49**, 2021–2036 (2007).
41. Uebel, M. et al. Fabrication of robust reference tips and reference electrodes for Kelvin probe applications in changing atmospheres. *Langmuir* **33**, 10807–10817 (2017).
42. Leng, A., Streckel, H. & Stratmann, M. The delamination of polymeric coatings from steel. Part 1: calibration of the Kelvin probe and basic delamination mechanism. *Corros. Sci.* **41**, 547–579 (1999).
43. Han, S.-J., Yoo, M., Kim, D.-W. & Wee, J.-H. Carbon dioxide capture using calcium hydroxide aqueous solution as the absorbent. *Energy Fuels.* **25**, 3825–3834 (2011).
44. Rohwerder, M., Isik-Uppenkamp, S. & Stratmann, M. Application of SKP for in situ monitoring of ion mobility along insulator/insulator interfaces. *Electrochim. Acta* **54**, 6058–6062 (2009).
45. Posner, R., Wapner, K., Stratmann, M. & Grundmeier, G. Transport processes of hydrated ions at polymer/oxide/metal interfaces. Part 1. Transport at interfaces of polymer coated oxide covered iron and zinc substrates. *Electrochim. Acta* **54**, 891–899 (2009).
46. Posner, R. Ozcan, O. & Grundmeier, G. in *Design of Adhesive Joints Under Humid Conditions* (eds da Silva, L. F. M. & Sato, C.) (Spriger, Berlin Heidelberg, 2013).
47. Davantes, A. & Lefevre, G. In situ real time infrared spectroscopy of sorption of (poly)molybdate ions into layered double hydroxides. *J. Phys. Chem.* **117**, 12922–12929 (2013).

Open Access This article is licensed under a Creative Commons Attribution 4.0 International License, which permits use, sharing, adaptation, distribution and reproduction in any medium or format, as long as you give appropriate credit to the original author(s) and the source, provide a link to the Creative Commons license, and indicate if changes were made. The images or other third party material in this article are included in the article's Creative Commons license, unless indicated otherwise in a credit line to the material. If material is not included in the article's Creative Commons license and your intended use is not permitted by statutory regulation or exceeds the permitted use, you will need to obtain permission directly from the copyright holder. To view a copy of this license, visit http://creativecommons.org/licenses/by/4.0/.

© The Author(s) 2019